# Structural study of the zinc and cadmium complexes of a type 2 plant (Quercus suber) metallothionein: Insights by vibrational spectroscopy

**ARTICLE** *in* BIOPOLYMERS · JUNE 2007

Impact Factor: 2.39 · DOI: 10.1002/bip.20729 · Source: PubMed



**5 AUTHORS**, INCLUDING:

Anna Tinti
University of Bologna
**112** PUBLICATIONS **1,350** CITATIONS
SEE PROFILE

Merce Capdevila
Autonomous University of Barcelona
**99** PUBLICATIONS **1,849** CITATIONS
SEE PROFILE

Silvia Atrian
University of Barcelona
**123** PUBLICATIONS **3,295** CITATIONS
SEE PROFILE

Armida Torreggiani
Italian National Research Council
**88** PUBLICATIONS **1,104** CITATIONS
SEE PROFILE

# Structural Study of the Zinc and Cadmium Complexes of a Type 2 Plant (Quercus suber) Metallothionein: Insights by Vibrational Spectroscopy

Jordi Domènech,[1,2] Anna Tinti,[3] Mercè Capdevila,[4] Silvia Atrian,[1] Armida Torreggiani[2]

[1] *Departament de Genètica, Facultat de Biologia, Universitat de Barcelona, Av. Diagonal 645, 08028 Barcelona (Spain)*

[2] *ISOF, Consiglio Nazionale delle Ricerche, Via P. Gobetti 101, 40129 Bologna, Italy*

[3] *Biochemistry Department, University of Bologna, Via Belmeloro 8/2, 40126 Bologna, Italy*

[4] *Departament de Química, Facultat de Ciències, Universitat Autònoma de Barcelona, 08193 Barcelona (Bellaterra), Spain*

*Received 22 January 2007; revised 14 March 2007; accepted 17 March 2007*
*Published online 21 March 2007 in Wiley InterScience (www.interscience.wiley.com). DOI 10.1002/bip.20729*

## ABSTRACT:

*Zn- and Cd-complexes of Quercus suber metallothionein (QsMT) were obtained by in vivo-synthesis, in order to obtain physiologically representative aggregates, and characterized by spectrometric and spectroscopic methods. The secondary structure elements and the coordination environments of the metal binding sites of the two aggregates were determined, as well as the main metal-containing species formed. The results obtained from the analysis of the Raman and IR spectra reveal that these metal-MT complexes predominantly contain β-sheet elements (about 60%), whereas they lack α-helices. These structural features slightly depend on the divalent metal bound. In particular, $Cd^{II}$ binding to QsMT induces a slight increase of the β-sheet percentage, as well as a decrease in β-turn elements with respect to $Zn^{II}$ binding. Conversely, the in vivo capability of QsMT to inglobe metal and sulfide ions is metal-depending. Spectroscopic vibrational data also confirm the presence of sulfide ligands in the metal clusters of both Zn- and Cd-QsMT, while the participation of the spacer His residue in metal coordination was only found in Cd-QsMT, in agreement with the CD results. Overall data suggest different coordination environments for $Zn^{II}$ and $Cd^{II}$ ions in QsMT. © 2007 Wiley Periodicals, Inc. Biopolymers 86: 240–248, 2007.*

*Keywords:* *metallothionein; sulfur ligand; Raman spectroscopy; IR spectroscopy; metal complexes*

*Correspondence to:* Dr. Armida Torreggiani; e-mail: torreggiani@isof.cnr.it
Contract grant sponsor: Spanish Ministerio de Ciencia y Tecnología
Contract grant numbers: BIO2006-14420-CO2-01, BIO2006-14420-CO2-02



*This article was originally published online as an accepted preprint. The "Published Online" date corresponds to the preprint version. You can request a copy of the preprint by emailing the Biopolymers editorial office at biopolymers@wiley.com*

## INTRODUCTION

Metallothioneins (MTs) are low-molecular-weight cysteine-rich proteins characterized by their ability to coordinate both essential ($Zn^{II}$ and $Cu^{I}$) and xenobiotic ($Cd^{II}$ and $Hg^{II}$) metal ions.[1] Metal-MT coordination is mainly achieved by formation of metal-thiolate clusters, but the participation of nonproteic ligands, such as chloride and sulfide anions, has also been reported.[2,3] The striking combination of high thermodynamic but low kinetic stability is one of the main features of the metal-MT complexes that allow them to bind metals very tightly, and promptly exchange them to other proteins.[4] Because of these peculiar properties, the MT functional role has been related both to physiological metal homeostasis and to xenobiotic metal detoxification processes.[5]

MTs are widely distributed among the animal and plant kingdoms, although showing a high heterogeneity of sequence. Plant differ from animal MTs by a peculiar amino acid sequence organization consisting of two short cysteine-


**FIGURE 1** Amino acid sequence of the Type 2 plant MT from Quercus suber (QsMT). Cys and His residues are in bold.

rich terminal domains (containing from 4 to 8 Cys residues each) linked by a cysteine-devoid spacer region (30–50 residues). The length of this region and the distribution of the Cys residues are the basis of further classification of plant MTs in four types.[6] In contrast with the current knowledge on the 3D structure of animal MTs,[7–9] there is an appalling lack of structural data on plant MTs. Consequently, there are no information available about the contribution of their cysteine-rich domains and the spacer to the final metal-MT conformation. Attempts to propose a general fold for plant MTs have led to two main studies on *Actinia chinensis* and *Triticum aestivum* MTs which support the functional independence of the Cys-rich domains, and propose a dumbbell model similar to that reported for mammalian MT.[10,11] This model is also supported by the two-step dynamics observed during acid-induced $Cd^{II}$ release from *Fucus vesiculosus* MT.[12] On the other hand, studies on recombinant Cd-MT aggregates of *Pisum sativum*[13] support a hairpin model with the two Cys-rich domains conforming a unique metal cluster.

The plant Quercus suber MT (QsMT) has one spacer region flanked by two Cys-rich domains of 8 and 6 Cys respectively (Figure 1), and contains an additional putative ligand (His).[14] Our previous characterization of the Zn- and Cd-binding abilities of QsMT and its separate domains support the dependence of the two Cys-rich domains,[15,16] together with the participation of the spacer region in the in vivo folding of Zn- and Cd-QsMT, and in overcoming Cd toxicity in yeast.[16]

The comparative study of the Zn- and Cd-QsMT aggregates has indicated differences in their metal and sulfide content, suggesting structural differences depending on the metal coordination,[14,16] in contrast with the isomorphism commonly assumed for animal MTs.[17]

Raman and IR spectroscopies are powerful techniques to estimate the content of secondary structure elements in proteins and are very informative on metal-ligand coordination sites.[18–20] Despite the well-known potentialities of these techniques, to our knowledge they have been scarcely used in MT conformational studies. Thus, to further analyze the role of the spacer in QsMT folding and the structural differences between Zn- and Cd-QsMT aggregates that can be foreseen from their dissimilar metal-to-protein content,[14] a comparative Raman and IR study was carried out on the in vivo-synthesized QsMT metal aggregates. Hence, this work includes a detailed spectroscopic study of the Zn- and Cd-QsMT complexes, highlighting the individuation of Raman marker bands associated to the metal-QsMT clusters. The participation of peptidic donor groups (S-thiol and N-imidazol) and nonproteic ligands (as sulfide anions) in metal chelation, as well as secondary structure elements, were analyzed. The results are discussed, together with other functional data previously obtained,[14,16] in order to deepen in the folding model of plant MTs.

## EXPERIMENTAL

### Preparation and Characterization of the Zn- and Cd-QsMT Complexes

To produce the QsMT recombinant protein, 3.0 l of fresh LB medium were inoculated with 300 ml of an overnight culture of *E.coli* BL21 cells carrying the plasmide pGEX-QsMT, which consists on the pGEX vector with the cDNA of QsMT cloned in frame immediately downstream of the GST-coding region.[14] Induction with isopropyl $\beta$-D-thiogalactopyranoside (IPTG) was performed at $OD_{600} = 0.8$, and cultures were grown for a further 3 h in the presence of either 300 $\mu M$ $ZnCl_2$ or 300 $\mu M$ $CdCl_2$. Cells were lysed by sonication in the presence of 0.5% $\beta$-mercaptoethanol to prevent protein oxidation. From this step onwards, all procedures were carried out in argon-saturated buffers. After sonication, cellular debris was pelleted by centrifugation and the protein was isolated from the supernatant by affinity chromatography using Glutathione-Sepharose 4B (Amersham Pharmacia). QsMT was finally purified by fast performance liquid chromatography (FPLC) using a Superdex75 column (Pharmacia) equilibrated with 50 m$M$ Tris-HCl, pH 7.0.

The S, Zn and Cd contents were measured in the two metal-QsMT preparations by acid inductively-coupled plasma atomic emission spectroscopy (acid ICP-AES). A Polyscan 61 E Thermo Jarrell Ash spectropolarimeter was used, measuring S at 182,040 nm, Zn at 213,856 nm, and Cd at 228,802 nm.[2] The mean sulfide/protein content was estimated from gas-chromatography determinations (GC-FPD) performed in a HP Serie II gas chromatograph coupled to a flame photometric detector FPD80 CE Instruments (Thermo Finnigan).[2] Protein concentration was estimated from the S content, assuming that all S atoms in the samples were contributed by QsMT, that is 17 S atoms per mol QsMT (14 from Cys and 3 from Met residues). This method includes acidification of the samples with 1$M$ HCl prior to the ICP-AES analysis to favor the loss of the acid-labile ligands as $H_2S$ and thus ensure that all the sulfur remaining in the sample corresponded to Cys and Met.

Circular dichroism (CD) analyses were carried out in a Jasco spectropolarimeter (Model J-715) interfaced to a computer (J700 Software). All CD spectra of the samples in Tris-HCl (pH 7.0) were recorded in 1 cm capped quartz cuvettes, corrected for the dilution effects,[21] and processed using the program J810.

**Table I Analytical Characterisation of the Zn- and Cd-QsMT Preparations**

| Samples | Protein Concentration[a] | Metal Per Protein[a] | Sulfide ($S^{2-}$) Per Protein[b] | Species[c] |
|---|---|---|---|---|
| Zn-QsMT | $1.5 \times 10^{-4} M$ | 3.5 | 1 | **$Zn_4$-QsMT** |
| | | | | $Zn_4S_2$-QsMT |
| Cd-QsMT | $2.1 \times 10^{-4} M$ | 5.6 | 3 | **$Cd_6S_4$-QsMT** |
| | | | | $Cd_5$-QsMT |

[a] QsMT concentration and metal ratio calculated from the S, Zn, and Cd acid ICP-AES measurements, considering that each mol of recombinant QsMT accounts for 17 mol of S.

[b] Sulfide-to-QsMT ratio measured by GC-FPD.

[c] Molecular species detected by ESI-MS. Major species are represented in bold.

The molecular mass of the metal-peptide species was determined by electrospray ionization mass spectrometry (ESI-MS) performed in a Fisons Platform II instrument (VG Biotech) following the conditions previously described.[15] Briefly, 10 ml of the sample were injected through a PEEK column (1 m × 0.168 mm i.d.) at 20 $\mu$l $min^{-1}$ under the following conditions: source temperature 120°C, capillary-counterelectrode voltage 3.5 kV, lens-counterelectrode voltage 1.5 V, cone potential 60 V. The liquid carrier was a 20:80 (v/v) mixture of acetonitrile and 5 m*M* ammonium acetate, pH 7.0.

### Raman and Infrared Spectroscopic Analysis of Zn- and Cd-QsMT Aggregates

To obtain samples suitable for the FT-Raman and FTIR analyses, overcoming the spectroscopic masking effect of the Tris buffer, a dialysis-lyophilization protocol was set up. 1 ml of the Zn- and of the Cd-QsMT samples, containing about 1 mg of QsMT, were subjected to a 6-h dialysis against 200 ml of 5 m*M* Tris buffer at pH 7.0, using 6.3 mm-diameter dialysis membranes (Medicell International). Fresh Tris solution was provided every 2 h. Afterwards, the samples were frozen at −80°C for 1 h and lyophilized again. They were redissolved in 200 $\mu$l of deionised water, and submitted to an additional dialysis-lyophilization cycle. The maintenance of the global fold of the metal complexes was verified by checking their mean metal content and the chiroptical features after this treatment.

FT-Raman spectra were obtained on lyophilized samples in a Bruker IFS 66 spectrometer equipped with a FRA-106 Raman module and a cooled Ge-diode detector. The excitation source was a $Nd^{3+}$-YAG laser (1064 nm) in the backscattering configuration. The spectral resolution was 4 $cm^{-1}$ and the total number of scans for each spectrum was 6000 to facilitate the observation of the weaker features of the spectra and to improve the signal/noise ratio, in particular in the 800–200 $cm^{-1}$ region, critical for the S-participated bonds. Laser power was about 100 mW.

The FTIR spectra were obtained using a Nicolet 5700 FTIR spectrophotometer with a spectral resolution of 4 $cm^{-1}$ using the ATR technique. 1000 scans for each spectrum were accumulated and computer averaged for each sample.

The derivative spectra were calculated according to the Savitzky-Golay method. The curve fitting analysis was implemented using OPUS/IR v.2.0 program, with the Levenberg-Marquardt algorithm. In order to fit the vibrational bands, the positions and the bandwidth at half-height of the component peaks should be fixed or constrained within reasonable limits. A realistic identification of the peak component number and position was carried out by the fourth-derivative spectra, smoothed with a thirteen-point Savitsky-Golay function. These band positions were used as the initial guess for the curve-fitting of the original spectra. Best curve fitting were obtained at the lowest possible $\chi^2$ values. The IR component profiles used in the curve-fitting were described as Gaussian functions.

## RESULTS AND DISCUSSION

### Characterization of Zn- and Cd-QsMT Synthesized In Vivo

The metal complexes of QsMT biosynthesized in Zn- or Cd-enriched media were analyzed and characterized by spectroscopic and spectrometric methods. The average metal ion and acid-labile sulfide content ($S^{2-}$) of the recombinant QsMT preparations resulted to be higher in Cd-QsMT than in Zn-QsMT (Table I), consistently with the data previously reported for Zn-QsMT and Cd-QsMT aggregates.[14,16] These different metal stoichiometries that QsMT achieves when recombinantly synthesized (6 Cd towards 4 Zn), as well as the higher sulfide content of Cd-QsMT than Zn-QsMT, suggest the formation of different metal cluster structures.

Significant structural differences between the Zn- and Cd-QsMT aggregates were also revealed by the comparison of their CD spectra. In fact, the low-chirality CD profile of Zn-QsMT, with an exciton coupling at ca. 240 nm, as expected for a Zn-MT complex,[21] differed from that of Cd-QsMT that displayed two main absorptions: a Gaussian band at ca. 275 nm and a shoulder at about 250 nm (Figure 2). The first informs about the participation of sulfide ligands in the Cd-MT complexes,[2] whereas the second has been attributed to the involvement of His in the otherwise tetrahedral $Cd(SCys)_4$ chromophores.[16,22,23]

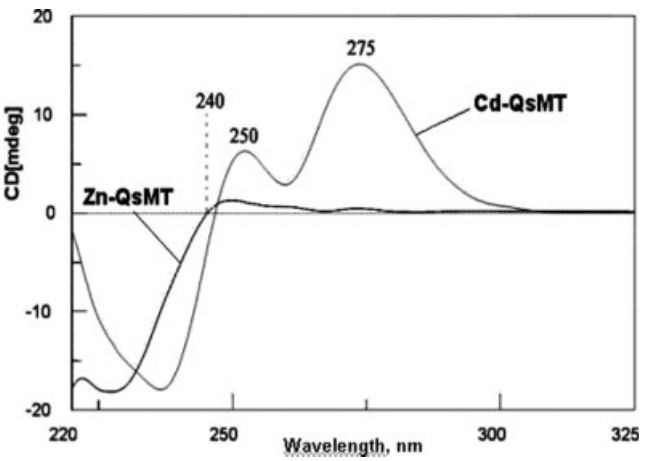


**FIGURE 2** CD spectra of Zn-QsMT and Cd-QsMT.

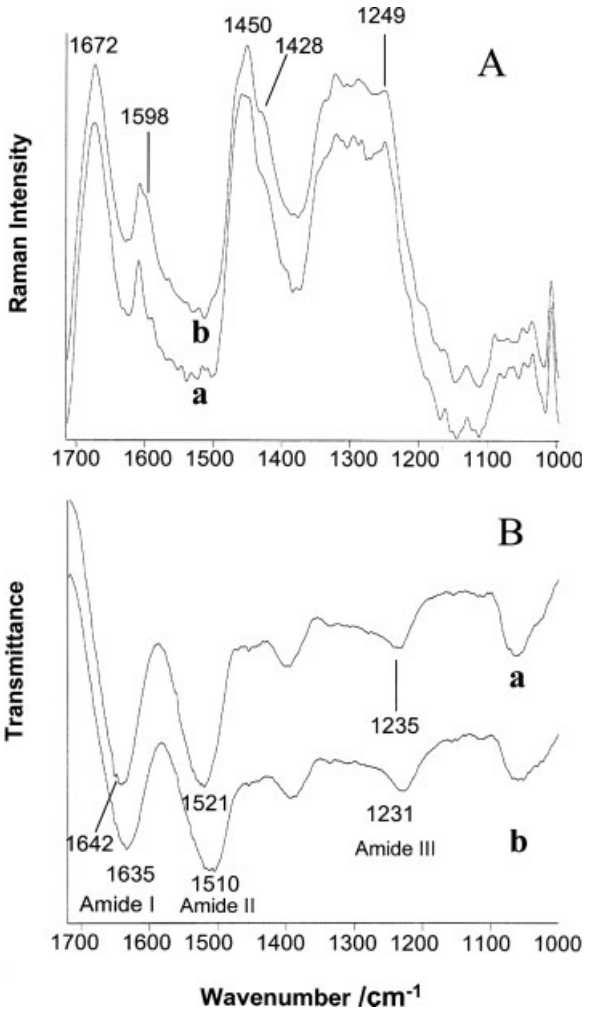


**FIGURE 3** Raman (A) and IR (B) spectra of Zn-QsMT (a) and Cd-QsMT (b) in the 1720–1000 $cm^{-1}$ range.

The ESI-MS measurements accounted for the presence of $S^{2-}$ ions as additional ligands, indicating that the synthesis of QsMT in Zn- or Cd-supplemented media leads to the formation of coexisting sulfide-containing and sulfide-devoid metallated species (Table I). In particular, the major species identified in Cd-QsMT contains 6 Cd(II) ions with participation of sulfide ligands (4 $S^{2-}$), whereas Zn-QsMT presents a clearly lower metal and sulfide content. Thus, these results suggest that QsMT in vivo exhibits distinct Zn(II)- and Cd(II)-binding capability.

## Secondary Structure Analysis

Raman spectroscopy advantages in the study of proteins lie in the correlation between the vibrational frequencies of the peptide backbone and the various protein conformations.[18–20] In particular, the amide I and III Raman bands, arising from the Raman-active vibrational modes of the CONH peptidic bond (C═O stretching and N—H in plane deformation, respectively), act as conformation sensitive markers. The Raman spectra of Zn- and Cd-QsMT in these regions are shown in Figure 3A, and Table II includes an assignment of their main bands. In both cases a strong amide I band centered at 1672 $cm^{-1}$ was visible, indicating the predominance of $\beta$-sheets in the metal-QsMT secondary structure.[20]

The comparison of the two spectra revealed some significant differences, such as the intensity of the amide III band and the presence of the band at $\approx$1600 $cm^{-1}$ due to His vibration. In particular, the $Zn^{II}$ binding to QsMT renders a slightly lower intensity of the amide III component at 1249 $cm^{-1}$, indicating a minor $\beta$-sheet content in Zn-QsMT compared with that in Cd-QsMT.

To obtain a more accurate evaluation of the conformational changes due to different metal binding, the percentages of secondary structure elements were calculated by Alix and co-workers' method.[24] This methodology, based on an equation obtained through a multi-parametric analysis of the correlations between X-ray structural and spectroscopic Raman data from a large set of reference proteins, permits expressing the percentages of structural elements in a protein as a linear function of some parameters of the amide I Raman band. The calculated percentages of secondary struc-

**Table II Tentative Assignment of the Main Bands in the 1700–1000 $cm^{-1}$ Raman Spectral Region of the Zn- and Cd-QsMT Preparations**

| Raman Wavenumbers ($cm^{-1}$) | | |
|---|---|---|
| Cd-QsMT | Zn-QsMT | Assignments |
| 1672 vs | 1672 vs | Amide I |
| 1606 s | 1608 s | Phe |
| 1598 s, sh | — | His (Taut II) |
| 1466 s, sh | 1466 sh | $\delta CH_2$, $\delta CH_3$ |
| 1450 vs | 1454 vs, br | $\delta CH_2$, $\delta CH_3$ |
| 1428 s, sh | 1427 m, sh | $\nu COO^-$ |
| 1340 m, br | 1348 m, sh | $CH_2$ t/r (Gly) |
| 1335 s, sh | 1334 s, sh | $CH_2$ t/r (Ser, Lys) |
| 1322 vs | 1320 vs | $CH_2$ t/r (Ser, Lys, His) |
| 1303 s | 1310 sh | Amide III ($\beta$-turns, $\alpha$-helix) |
| 1287 vs | 1295 vs | Amide III ($\beta$-turns) |
| 1280 sh | 1282 vs | Amide III ($\beta$-turns) |
| 1262 sh | 1263 sh | Amide III (Random) |
| 1249 vs | 1249 s | Amide III ($\beta$-sheet) |
| 1238 sh | 1235 sh | Amide III ($\beta$-turns) |
| 1089 m | 1082 m | $\nu$C—N, $\nu$C—C |
| 1070 m | 1068 m | $\nu$C—N, $\nu$C—C |
| 1048 m | 1046 m | $\nu$C—N, $\nu$C—C |
| 1035 m | 1034 m | Phe |
| 1006 s | 1006 s | Phe |

Assignments: $\nu$, stretching; $\delta$, in plane bending; t/r, twist/rock. Intensities: w, weak; m, medium; s, strong; v, very; sh, shoulder.

**Table III Percentages of Secondary Structure Present in Zn-QsMT and Cd-QsMT Obtained by the Analysis of the Raman Amide I and IR Amide III Regions**

| | Percentages (%) | | | |
|---|---|---|---|---|
| | Zn-QsMT | | Cd-QsMT | |
| Conformation | Raman Data[a] | IR Data[b] | Raman Data[a] | IR Data[b] |
| α-Helix | 1 | 4 | 0 | 2 |
| β-Sheet | 61 | 55 | 64 | 58 |
| β-Turns | 24 | 26 | 22 | 24 |
| Random | 14 | 13 | 14 | 16 |

[a] Percentages obtained by method of Alix et al.[24]
[b] Percentages obtained by curve fitting method.

ture elements of QsMT complexes are shown in Table III. The amide I band analysis indicated a relevant contribution of β-sheet and β-turn segments, whereas the α-helix content resulted to be negligible. It is also evident that $Zn^{II}$ coordination slightly favors major content of β-turns and minor β-sheet content, in relation to Cd-QsMT, whereas it does not affect the percentage of disordered conformation, thus confirming the previous conclusions drawn from the qualitative spectrum analyses.

FT-IR spectra were also analyzed (Figure 3B). The three amide bands sensitive to conformations were significantly downshifted for Cd-QsMT, in respect to Zn-QsMT, suggesting a higher β-sheet content in the former than in the latter. The quantitative evaluation of the secondary structural elements was obtained by the analysis of the IR amide III region. In fact, the amide III band, although less intense than amide I band, facilitates the structural analysis of proteins since there is not interference of water bands in this region and allows for an easier deconvolution of the band components.[25–28]

The Gaussian curve fitting method based on a least-square fit of several curves to an experimental spectrum was applied (see Figure 4). An indication of the number and position of the fitting bands was obtained by the fourth-derivative spectra,[29] and the secondary structure element content were calculated from the integrated intensities of the individually assigned bands and their fraction of the total intensity.[20,30] Although this method does not yield the absolute content of the secondary structures (since the effective intensities of the bands corresponding to different structure elements are not completely equivalent), it may be used to demonstrate protein conformational changes induced by external factor interaction, such as metal binding.

The IR spectra of the two metal complexes of QsMT exhibited eight components in the 1205–1320 $cm^{-1}$ region, resulting from the contribution of different secondary structure elements.[20,30] Four components attributable to β-sheet conformation appeared in the 1207–1245 $cm^{-1}$ range, one component at about 1257 $cm^{-1}$ was attributable to random conformation, and one-two component(s) reflected the contribution of β-turns and α-helix, respectively.

The results from this curve fitting analysis (Table III) allow comparison between the two methods used. The percentages of unordered conformation (β-turns and random coil) obtained by the two methods compare fairly well, while the α-helix and β-sheet content appear to be respectively slightly overestimated and underestimated by the curve fitting method with respect the Alix's method. This suggests that a systematic error is present in one of the two methods. However, the interpretation of all the experimental data is not significantly dependent on the method used, and both Zn- and Cd-QsMT aggregates appear to be predominantly contributed by β-sheets with almost complete exclusion of α-helices. This important β-sheet contribution is fairly rare

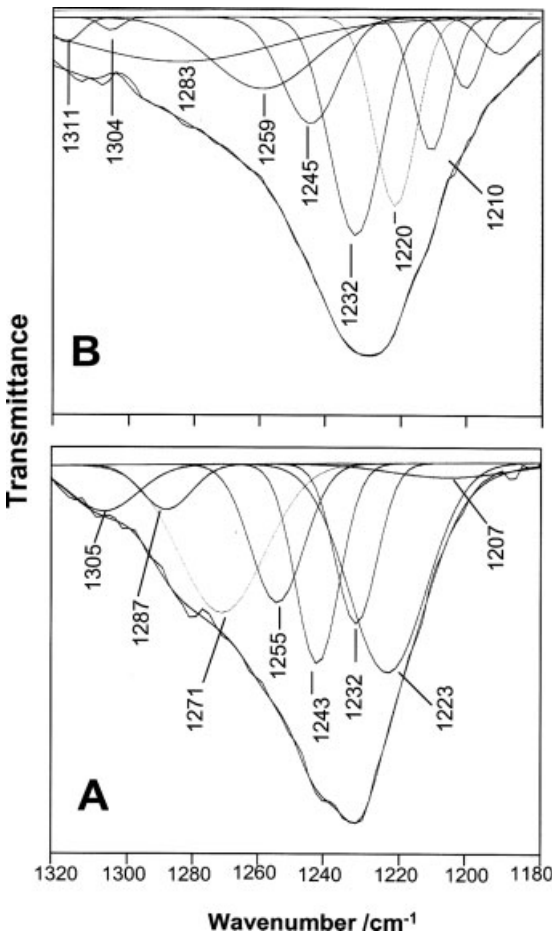


**FIGURE 4** Curve fitting analysis of the amide III bands of the IR spectra of Cd-QsMT (A) and Zn-QsMT (B).

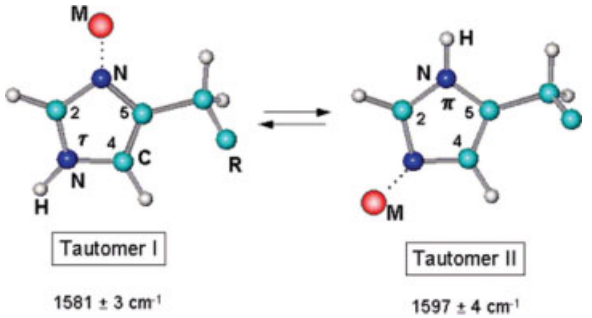


**FIGURE 5** Histidine tautomeric forms and Raman wavenumbers related to metal binding.

among MTs. The Chou and Fasman prediction method[31] assigns the highest score for $\beta$-sheet conformation to a segment encompassing Thr35 to Lys47, a central stretch in the spacer region of QsMT. The whole spacer region constitutes nearly the 50% of the polypeptide, and therefore is a good candidate to adopt a $\beta$-sheet fold that would not be distorted by metal coordination, while the Cys-rich regions accumulate the highest scores for $\beta$-turn prediction by this same method.[31]

Overall, it can be concluded that the Zn- and Cd-QsMT secondary structure is composed mainly by $\beta$-sheets, probably located in the spacer region, and $\beta$-turns conforming the cysteinic regions. This distribution fits well with the 3D structures reported for several MT complexes,[32] which rarely exhibit structures other than $\beta$-turns. This is in concordance with the observation that other secondary structures ($\alpha$-helices or $\beta$-sheets) are prevailingly restricted to amino acid sequences devoid of Cys, and thus very rare in prokaryotic and animal MTs.[33,34]

## Metal Binding Environment and Coordination Sites

The two nitrogen atoms of the QsMT His residue are potential donors for transition metal ions and its coordination can be detected by using Raman marker bands such as the $C_4{=}C_5$ stretching band. In fact, this band appears at different wavenumbers depending if $N_\tau$ or $N_\pi$ binds to metal ions (see Figure 5).[35–37] Thus, although His Raman bands are weak when compared to those of aromatic amino acids, their identification is possible in proteins with a low content of Tyr or Phe, such as MTs (i.e. 0 Tyr and 2 Phe in QsMT).[38]

In the Cd-QsMT Raman spectrum, a band at 1598 $cm^{-1}$ was clearly visible, whereas only a very weak shoulder appeared at this wavenumber for Zn-QsMT (Figure 3A). The presence of this band, attributable to His tautomer II ($N_\pi$—H), energetically less stable than I, suggests that $N_\tau$-imidazole takes part in the $Cd^{II}$ binding,[39–41] in concordance with the CD data suggesting His participation in Cd binding. The same tautomeric form of His has been found to be involved in metal-binding in metalloproteins such as hemoglobin and in *Clostridium pasteurianum* iron hydrogenases.[42–44]

As far as cysteinic sulfurs are concerned, almost all Cys residues present in QsMT (14 Cys) are involved in the metal coordination, as indicated by the absence of the Raman band at $\approx$2570 $cm^{-1}$ due to free —SH groups and the weak contribution of disulfide stretching vibrations (500–540 $cm^{-1}$ region) (Table IV).

The Raman region from 200 to 800 $cm^{-1}$ provides useful information about the bonds in which sulfur atoms participate, although the presence of some backbone skeletal vibration bands.[18,45,46] In particular, the absence of Trp residues, which originate bands in this region, allows a deeper analysis of the $\nu$S—S, $\nu$C—S, and $\nu$M—S spectral regions of metal-QsMT (Figure 6 and Table IV).

The involvement of both the Cys sulfur atoms and the sulfide anions in metal binding in Zn- and Cd-QsMT is clearly

**Table IV Tentative Assignment of the Main Bands in the 800–200 $cm^{-1}$ Raman Spectral Region of the Zn- and Cd-QsMT Preparations**

| Raman wavenumbers ($cm^{-1}$) | | |
|---|---|---|
| Cd-QsMT | Zn-QsMT | Assignments |
| — | 778 sh | $rCH_2$ |
| 760 m | 763 m | $\nu$C—S, amide V, $\gamma$NH |
| 723 w, sh | 725 w | $\nu$C—S (Met) |
| 700 sh | 705 sh | $\nu$C—S (Met) |
| — | 688 w | $\nu$C—S |
| 680 w | 673 w | $\nu$C—S |
| 655 sh | 660 w | $\nu$C—S |
| 624 w | 624 w | Phe |
| 530 vw | 520 w | $\nu$S—S, $\delta$CCC(Val) |
| 505 vw | 510 w | $\nu$S—S |
| 447 vw | — | $\nu$M—S, dCCN |
| 424 sh | 423 w, sh | $\nu$M—$S_b$—M |
| 417 m | 418 w | $\nu$M—$S_b$—M |
| 405 vw, sh | 405 vw, sh | $\nu$M—S, dCCN |
| 392 vw, sh | 390 vw | $\nu$M—S, dCCN |
| 368 vw, | 369 vw, br | $\nu$M—S |
| — | 342 w | $\nu$M—S |
| 333 sh | 328 w, sh | $\nu$M—S |
| 319 w, sh | 319 w, sh | $\nu$M—S, dCCN |
| — | 311 w | $\nu$M—S |
| 305 m | — | $\nu$M—S, dCCN |
| 289 m | 284 vw | $\nu$M—S, amide VI |

Assignments: $\nu$, stretching; $\delta$, in plane bending; $\gamma$, out of plane bending; r, rocking; d, skeletal deformation. Intensities: w, weak; m, medium; s, strong; v, very; sh, shoulder; br, broad. $S_b$, bridging sulfur; M, metal.

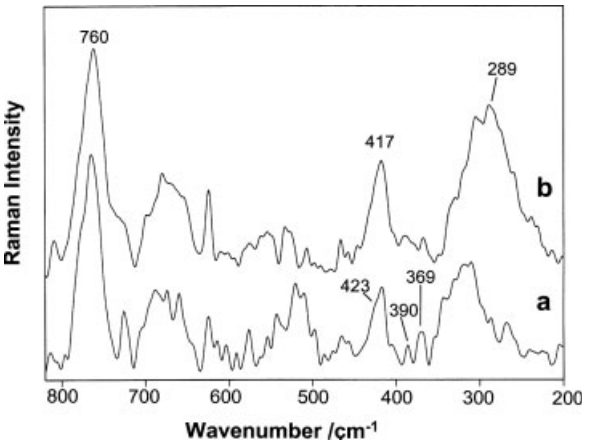


**FIGURE 6** Raman spectra of Zn-QsMT (a) and Cd-QsMT (b) in the 820–200 $cm^{-1}$ range.

visualized in the Raman spectra from the presence of several bands attributable to the metal-S stretching modes at low wavenumbers (<500 $cm^{-1}$).[37,47–49] In particular, the high number of the *ν*M-S bands, as well as their broadening, (Table IV) suggest the formation of different metal centers both in Zn- and Cd-QsMT. This finding is in agreement with the ESI-MS results, indicating the coexistence in both sample of sulfide-containing and sulfide-devoid metal-MT species whose predominance is metal-depending.

The Raman spectrum of Cd-QsMT showed a more intense 417 $cm^{-1}$ band than that of Zn-QsMT (Figure 6). A similar band, although the presence of a different metal (Fe instead of Zn), was visible in the Raman spectra of [2Fe-2S] and Rieske ferredoxins, two metalloproteins with the "unusual" characteristic to have metal ions bound by bridging sulfide anions and terminal cysteine ligands[46,50]; in that case the band at 410–420 $cm^{-1}$ has been assigned to the M-$S_b$-M bond vibrations ($S_b$ standing for bridging sulfur, and M for metal). This assignment well agrees with the different sulfide content revealed in our samples (Table IV): the higher band intensity would be consistent with a more important participation of the sulfur bridging ligands in the former, in accordance with the analytical data reported in Table I. Thus, this Raman band, which appears to be poorly affected by the nature of the metal, could be considered a marker of sulfur-atom bridging ligands.

Other bands related to sulfur-metal bonds fall in the 250–370 $cm^{-1}$ region (Table IV) and suggest the presence of different metal cluster geometry in the two metallated QsMT, in

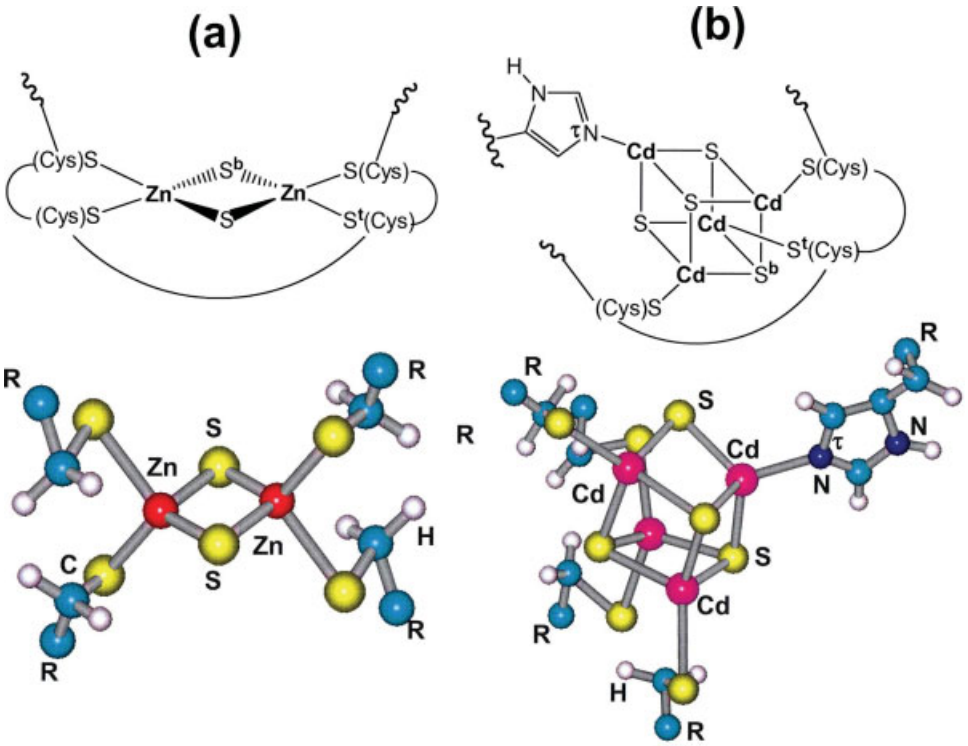


**FIGURE 7** Different geometry of metal clusters where sulfur-atom bridging ligands are involved: (A) binuclear- and (B) cubane-type. $S_b$, bridging sulfur (from sulfide anions or Cys); $S_t$, terminal sulfur (from Cys). At the bottom: optimized nuclear configuration of the $Zn_2S_2$ and $Cd_4S_4$ cluster cores proposed to exist in Zn- and Cd-QsMT. Optimization was performed by using Hyper-Chem v. 4 semi-empirical method ZINDO/1. To obtain a model simplification, the protein chain was indicated as R.

addition to metal centers ($MS_4$) with a probable tetrahedral geometry.[49,51,52] In particular, a cubane-type cluster for $Cd^{II}$ ions could be suggested by the 289 $cm^{-1}$ band, in addition to the 330 and $\approx$420 $cm^{-1}$ shoulders, visible in the Cd-QsMT spectrum,[51] whereas a binuclear Zn-S centre could be present in Zn-QsMT on the basis of the similarity of the Raman bands at 284, 328, 342, 369, 390, and 423 $cm^{-1}$ with those observed for the [2Fe-2S] ferredoxin (282, 327, 340, 367, 395, and 426 $cm^{-1}$) (see Figure 7).[50]

The geometric optimization of the molecular structures of the proposed metal centers involving bridging ligands was performed by semiempirical method ZINDO/1 (see Figure 7). A quasi-planar geometry and a distorted cube with the sides of unequal length resulted for $Zn_2S_2$ and $Cd_4S_4$ cores, respectively, whereas a quasi-tetrahedral geometry was assumed by each metal ions.

The C—S stretching modes originated from Cys, Met, and cystines cover a wide range of wavenumbers (from 650 to 780 $cm^{-1}$) since they depends on the conformational environment of the C—S bond. Zn- and Cd-QsMT Raman spectra showed a band at ca. 760 $cm^{-1}$ attributable to *ν*C-S, peculiar of metal-MT complexes (see Figure 6).[46] The fourth-derivative spectra of this region evidenced the presence of three components ($\approx$774, $\approx$764, and $\approx$757 $cm^{-1}$) of which the two low wavenumber components can be attributed to *ν*C-S of metal-Cys bonds.[37] The curve fitting analysis of this band showed the predominance of the lowest wavenumber component in Zn-QsMT ($\approx$80%) and a minor contribution in Cd-QsMT ($\approx$40%). These results evidence a minor variability in the S-$CH_2$ bond geometry in the $Zn^{II}$ co-ordination environment in respect to that in Cd-QsMT, in concordance with the predominance of the $Zn_4$-QsMT species detected by ESI-MS measurements. The differences in alkyl side chain conformations were also confirmed by the slight spectral changes observable in the 1420–1480 $cm^{-1}$ Raman range where the $\delta CH_2/\delta CH_3$ bands are visible (Figure 3A).

In addition, the difference in size, electrostatic forces and covalent bonding forces of zinc and cadmium ions can well justify the presence of different coordination geometry. In particular, the smaller Zn ionic radius and shorter metal-S bond distance could result in a more compact structure and a reduced protein volume for Zn-QsMT compared to Cd-QsMT.

By considering all the spectroscopic results, as well as the different metal and sulfide content, the metal-S centers could be summarized in three main types. Firstly, a tetrahedron-type cluster present in both the two metallated QsMT forms, in agreement with the literature where this coordination geometry is extensively reported for other MTs[17]; second, coordination centers involving sulfur atom bridging ligands such as the binuclear- and cubane-types, present in Zn- and Cd-QsMT, respectively.

## CONCLUSION

Raman and IR spectra of Zn- and Cd-QsMT complexes indicate the presence of secondary structural elements. The high *β*-sheet percentage in the secondary structure of these species is to our knowledge fairly rare among MTs. From our *in silico* studies on the QsMT sequence, it can be stated that the *β*-sheet elements would be situated mainly in the long Cys-devoid spacer, characteristic of most plant MTs.

The amount of secondary structure elements present in QsMT experiments only slightly changes depending on metal (Zn or Cd), in contrast with essential differences regarding the composition and geometry of the Zn- and Cd-clusters (oppositely to what is commonly accepted for MTs). In fact, Zn-QsMT mainly folds in a structure enclosing four Zn(II) ions and a low number of sulfide ligands with no participation in metal co-ordination of His residue, whereas a higher number both of Cd(II) and sulfide ions, as well as the His residue in the spacer region, are involved in the main Cd-QsMT structure. In addition, the finding that QsMT is capable to bind a higher content of Cd in comparison to Zn is also of interest since it suggests that this protein could play an important role in the heavy metal plant detoxification.

Sulfide-containing complexes, in addition to the expected nonsulfide-containing canonical species, were revealed in both Zn(II) and Cd(II) aggregates. This finding is worth considering since $S^{2-}$ ion is a species not restricted to *E.coli* but rather a universal cell component and its presence can be connected with physiological events which have also been proposed as functions for MTs (i.e. redox equilibrium).[4]

Finally, this study demonstrates again the power of Raman and IR spectroscopy for investigating protein secondary structures and the interaction of the amino acid side chains with metal ions. In fact, the use of these spectroscopies has been useful to approach unambiguously in QsMT three basic structural points poorly described until now in MTs: the participation of His residues to metal binding, the presence of secondary structure elements and the participation of sulfide ions to the metal-coordination sphere. Thus, equivalent studies with other MT forms are being performed to expand the vision on MT structure and functionality.

We are grateful to G. Mir and M. Molinas (Universitat de Girona, Spain), who kindly provided the pGEX-QsMT clone and Prof. C. Fagnano (University of Bologna, Italy) for the fruitful discussions on the Raman and IR results. We also thank the Serveis Científico-Tècnics de la Universitat de Barcelona for allocating instrument time.

## REFERENCES


1. Kägi, J. H. R. In Metallothionein III. Biological Roles and Implications; Suzuki, K. T.; Imura, N.; Kimura, M., Eds.; Birkhäuser Verlag: Basel, 1993; pp 29–55.
2. Capdevila, M.; Domenech, J.; Pagani, A.; Tio, L.; Villarreal, L.; Atrian, S. Angew Chem 2005, 44, 4618–4622.
3. Villarreal, L.; Tío, L.; Atrian, S.; Capdevila, M. Arch Biochem Biophys 2005, 435, 331–335.
4. Maret, W. Biochemistry 2004, 43, 3301–3309.
5. Palmiter, R. D. Proc Natl Acad Sci USA 1998, 95, 8428–8430.
6. Cobbett, C.; Goldsbrough, P. Annu Rev Plant Biol 2002, 53, 159–182.
7. Furey, W. F.; Robbins, A. H.; Clancy, L. L.; Winge, D. R.; Wang, B. C.; Stout, C. D. Experientia Suppl 1987, 52, 139–148.
8. Otvos, J. D.; Olafson, R. W.; Armitage, I. M. J Biol Chem 1982, 257, 2427–2431.
9. Riek, R.; Precheur, B.; Wang, Y.; Mackay, E. A.; Wider, G.; Guntert, P.; Liu, A.; Kagi, J. H.; Wuthrich, K. J Mol Biol 1999, 291, 417–428.
10. Zhu, C.; Lü, T.; Zhang, R.; Zhao, N.; Liu, J. Chin Sci Bull 2000, 45, 1413–1417.
11. Bilecen, K.; Ozturk, U. H.; Duru, A. D.; Sutlu, T.; Petoukhov, M. V.; Svergun, D. I.; Koch, M. H.; Sezerman, U. O.; Cakmak, I.; Sayers, Z. J Biol Chem 2005, 280, 13701–13711.
12. Merrifield, M. E.; Chaseley, J.; Kille, P.; Stillman, M. J Chem Res Toxicol 2006, 19, 365–375.
13. Kille, P.; Winge, D. R.; Harwood, J. L.; Kay, J FEBS Lett 1991, 295, 171–175.
14. Mir, G.; Domenech, J.; Huguet, G.; Guo, W. J.; Goldsbrough, P.; Atrian, S.; Molinas, M. J Exp Bot 2004, 55, 2483–2493.
15. Domenech, J.; Mir, G.; Hughet, G.; Molinas, M.; Capdevila, M.; Atrian, S. Biochimie 2006, 88, 583–593.
16. Domènech, J.; Orihuela, R.; Mir, G.; Molinas, M.; Atrian, S.; Capdevila. M. J Biol Inorg Chem, Submitted.
17. Kägi, J.; Kojima, Y. Metallothionein II. Proceedings of the 2nd International Meeting on Metallothionein and Other Low Molecular Weight Metal-Binding Proteins. Birkhäuser: Basel, 1987.
18. Tu, A. Raman Spectroscopy in Biology. Principles and Applications; Wiley-Interscience: NY, 1982.
19. Tuma, R. J Raman Spectr 2005, 36, 307–319.
20. Parker, F. S. Application of Infrared Raman and Resonance Raman Spectroscopy in Biochemistry; Plenum Press: NY, 1983.
21. Cols, N.; Romero-Isart, N.; Capdevila, M.; Oliva, B.; Gonzalez-Duarte, P.; Gonzalez-Duarte, R.; Atrian, S. J Inorg Biochem 1997, 68, 157–166.
22. Romero-Isart, N.; Cols, N.; Termansen, M. K.; Gelpi, J. L.; Gonzalez-Duarte, R.; Atrian, S.; Capdevila, M.; Gonzalez-Duarte, P. Eur J Biochem 1999, 259, 519–527.
23. Villarreal, L.; Tio, L.; Capdevila, M.; Atrian, S. FEBS J 2006, 273, 523–535.
24. Alix, A. J. P.; Pedanou, G.; Berijot, M. J Mol Struct 1988, 174, 159–164.
25. Byler, D. M.; Susi, H. Biopolymers 1986, 25, 469–487.
26. Wi, S.; Pancoska, P.; Keiderling, T. A. Biospectroscopy 1998, 4, 93–106.
27. Arrondo, J. L.; Muga, A.; Castresana, J.; Goni, F. M. Prog Biophys Mol Biol 1993, 59, 23–56.
28. Hollosi, M.; Majer, Z.; Ronai, A. Z.; Magyar, A.; Medzihradszky, K.; Holly, S.; Perczel, A.; Fasman, G. D. Biopolymers 1994, 34, 177–185.
29. Maddams, W. F; Southon, M. J. Spectrochim Acta A 1982, 38, 459–466.
30. Cai, S.; Singh, B. R. Biophys Chem 1999, 80, 7–15.
31. Chou, P. Y.; Fasman, G. D. Annu Rev Biochem 1978, 47, 251–276.
32. Gonzalez-Duarte, P. Comprehensive Coordination Chemistry II; McCleverty, J.; Meyer T. J., Eds.; Elsevier: Amsterdam, 2003.
33. Blindauer, C. A.; Harrison, M. D.; Parkinson, J. A.; Robinson, A. K.; Cavet, J. S.; Robinson, N. J.; Sadler, P. J Proc Natl Acad Sci USA 2001, 98, 9593–9598.
34. Wang, H.; Zhang, Q.; Cai, B.; Li, H.; Sze, H. K.; Huang, Z. X.; Wu, H. M.; Sun, H. FEBS Lett 2006, 580, 795–800.
35. Ashikawa, I.; Itoh, K. Biopolymers 1979, 18, 1859–76.
36. Takeuchi, H.; Kimura, Y.; Koitabashi, I.; Harada, I. J. Raman Spectrosc 1991, 22, 233–236.
37. Miura, T.; Satoh, T.; Takeuchi, H. Biochim Biophys Acta 1998, 1384, 171–179.
38. Miura, T.; Suzuki, K.; Kohata, N.; Takeuchi, H. Biochemistry 2000, 39, 7024–70.
39. Torreggiani, A.; Bonora, S.; Fini, G. Biopolymers 2000, 57, 352–364.
40. Torreggiani, A.; Tamba, M.; Bonora, S.; Fini, G. Biopolymers 2000, 57, 149–159.
41. Takeuchi, H. Biopolymers 2003, 72, 305–317.
42. Dickerson, R. E.; Gei, I. Hemoglobin; Benjamin/Cummings: Redwood City, CA, 1983.
43. Adams, M. W. Biochim Biophys Acta 1990, 1020, 115–145.
44. Peters, J. W.; Lanzilotta, W. N.; Lemon, B. J.; Seefeldt, L. C. Science 1998, 282, 1853–1858.
45. Overman, S. A.; Thomas, G. Biochemistry 1999, 38, 4018–4027.
46. Pande, J.; Pande, C.; Gilg, D.; Vasak, M.; Callender, R.; Kägi, J. H. Biochemistry 1986, 25, 5526–5532.
47. Han, S.; Czernuszewicz, R. R.; Kimura, T.; Adams, M. W. W.; Spiro, T. G. J Am Chem Soc 1989, 111, 3505–3511.
48. Boldyrev, A. I.; Simons. J Mol Phys 1997, 92, 365–379.
49. Adams, D. M.; Cornell, J. B. J Chem Soc A 1968, 1299–1303.
50. Rotsaert, F. J.; Pikus, J. D.; Fox, B. G.; Markley, J. L.; Sanders-Loehr, J. J Biol Inorg Chem 2003, 8, 318–326.
51. Lover, T.; Bowmaker, G. A.; Seakins, J. M.; Cooney, R. P. Chem Mater 1997, 9, 967–975.
52. Vargek, M.; Zhao, X.; Lai, Z.; McLendon, G. L.; Spiro, T. G. Inorg Chem 1999, 38, 1372–1373.


*Reviewing Editor: Laurence Nafie*